Chapter

Experimental and Theoretical Study of the Adsorption Behavior of Nitrate Ions by Layered Double Hydroxide Using Impedance Spectroscopy

Abderrahmane Elmelouky, Abdelhadi Mortadi, Elghaouti Chahid and Reddad Elmoznine

Abstract

This chapter analyzes the experimental data using impedance spectroscopy to reduce water pollution by nitrate ions. The adsorption is through a synthesized layered double hydroxide (Zn_3-Al-Cl-LDH). The kinetic study data analysis by pseudo-first-order and pseudo-second-order models is highly correlated they were found to fit very well the pseudo-second-order. This is confirmed by fast kinetic modeling of experimental data according to the pseudo-second-order. Furthermore, the Nyquist plots suggest that the grains and grain boundaries have contributed to the conduction mechanism of the material at different adsorption times and monitoring of the adsorption phenomenon. The investigation by impedance spectroscopy was used for modeling by an equivalent circuit. The real and imaginary functions of impedance complex are analyzed by modifying Cole-Cole relaxation. Revel most changes in the structure of the manifestation of the grains and the grains boundaries. The alternative current (AC) conductivity was investigated using the double power law of Jonscher. More importantly, the calculated value and the percentage of efficiency are evaluated in the adsorption. The water molecules and nitrate ions in the adsorbed were favored for the generation of the electrical response. The electrochemical impedance spectroscopy data are often interpreted by using electrical equivalent circuits.

Keywords: materials science, materials chemistry, impedance spectroscopy, layer charge, ionic, conductivity, dielectric

1. Introduction

Impedance spectroscopy is used to obtain an electrical equivalent circuit that showed the best fit of the experimental data. The analysis of these impedance data using both Bode and Nyquist plots was useful for the identification and the deconvolution of different processes of adsorption and interfaces. The adsorption-desorption phenomena representing the fundamental and essential electrochemical

processes at the solid-liquid interface and adsorption of ionic and nonionic surfactants on the solid/liquid interfaces have been studied experimentally [1–4] and theoretically [5–8]. The surface area of a solid electrode also affects adsorption efficacy [3]. On the other hand, the contamination of wastewater by nitrate ions has become an ever-increasing and serious environmental threat for a long time [9]. The disproportionate application of chemical products in industrial sectors causes the increases in large quantities of this ion into wastewater and surface water [10]. The solubility of the ions of nitrate is very high in water [11] is considered the most widespread contaminant exhibit a serious in this literature [12, 13]. The high amount of nitrate in drinking water can cause a number of health problems such as gastric cancer [14]. The methemoglobinemia or blue baby syndrome, a serious health danger, occurs when nitrate is converted to nitrite which then reacts with the hemoglobin to cause blueness of the skin of newborn infants; this is discussed by [15]. The superior costs of adsorption using adsorbents such as activated carbon prompt researchers to find other cheaper substitutes such as lamellar double hydroxides (LDH) which have been shown to be effective for the removal of this contaminant from industrial washing water [16–18]. Although studies have examined this material, its application toward the removal of nitrate has not been examined previously. Therefore, the present chapter is aimed to synthesize and to study the efficient removal of nitrate by LDH. This system has low-mobility charge carriers, which are believed to be responsible for the dielectric response.

2. Equipment and its use

2.1 Synthetic adsorbent and characterization techniques

The coprecipitation method was used to prepare Zn_3-Al-Cl-LDH described by [19], with constant pH (pH = 7) and molar ratio (R = Zn^{2+}/Al^{3+}). Pure $ZnCl_2$ (0.3 mol) and $AlCl_3.6H_2O$ (0.1 mol) solution with a molar ratio of R = 3 is dissociated in distilled water (250 mL) to produce solution (a) and solution (b) containing NaOH (0.8 mol) and NaCl (0.05 mol) in 250 mL of distilled water. After solution (b) is added to solution (a) with vigorous stirring at pH = 7 with an N_2 start to control contamination by carbonate ions. The precipitate was thoroughly washed with deionized water and dried at 60°C for 24 h to obtain the LDH of formula ($Zn_{2.93}$Al (OH) 7.86) (Cl^-. 1.87 H_2O noted Zn_3Al-Cl-LDH according to [20].

In the X-ray powder diffraction (XRD), the samples were recorded on an X-ray diffractometer (SIEMENS D 501) with a radiation of λKα1 = 1.5405 Å and λKα2 = 1.5444 Å. The patterns were recorded from 2° to 76° 2θ angles at a step size of 0.02° and at a speed of 5°/min.

The Perkin-Elmer 16 PC Fourier transform spectrometer (FTS) was used for infrared measurements. The samples were prepared in a pellet of 13 mm diameter and 1 mm thickness using 2 mg of product diluted in 200 mg of KBr. The FT-IR spectra were recorded in absorbance in the wave number range of 400–4000 cm^{-1} at 25°C with a resolution of 1 cm^{-1}.

The frequency range from 20 Hz to 1 MHz was performed for impedance spectroscopy measurements, with eight points per decade at room temperature utilizing an impedance analyzer (Hewlett Packard 4192A). The electrical contacts were performed using silver electrodes, which were deposited on the two circular faces of the sample [19]. The magnitude of the applied signal is 0.6 V peak to peak. An amount of 200 mg is pelleted to analyze the impedance [19]. The granulated powder was compacted under a hydraulic press with 250 MPa pressure into discs of 13 mm diameter and 1 mm thickness approximately [19]. The impedance spectra

were recorded at different adsorption times (5, 10, 20, 30, and 60 min). The analysis and theoretical fitting by impedance spectroscopy using complex empirical functions were carried out utilizing the software ZView 2.2 and Origin 8 for modeling of the ionic conductivity and the imaginary function according to the real function, respectively.

3. Results and discussion

3.1 X-ray diffraction

The X-ray diffraction patterns of Zn_3-Al-Cl-LDH depicted in **Figure 1** of the sample are characteristic to those of a double lamellar hydroxide. The sample was crystallized in a rhombohedral symmetry (space group: R-3m) with $(c/3) = d_{003} = 2d_{110}$ and $a = 2d_{006}$. The lattice parameters **c** and **a** are, respectively, 2.38 and 0.31 nm. These values are similar to those reported in the literature [14].

The peak (1 1 0) indicates the intermetallic distance used to calculate a lattice parameter (a = 2d110). Moreover, the values of the parameters **c** and **a** are, respectively, 23.82 and 3.10 A°. These values are similar to those reported in the literature [19].

3.2 Infrared spectroscopy

FT-IR confirms that the spectra of synthesized Zn_3Al-Cl-$(NO_3^-)_{ads}$-LDH (**Figure 2**) resemble those of hydrotalcite-like phases [21]. The FT-IR presents a close-up view of the most important regions of the infrared spectra of Zn_3Al-Cl-$(NO_3^-)_{ads}$-LDH depicted in **Table 1**.

The frequencies of absorbance links in this material are reported in **Table 1**. Indeed the infrared spectra of this material after adsorption at a different time show the increase in the intensity of characteristic link of NO_3^- ions at 1381 cm^{-1} as a function of time.

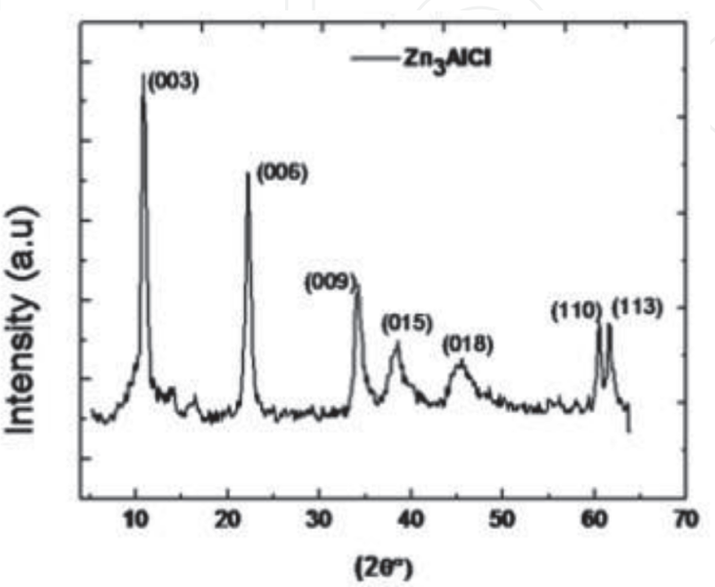

Figure 1.
XRD pattern of Zn_3-Al-Cl-LDH-blank.

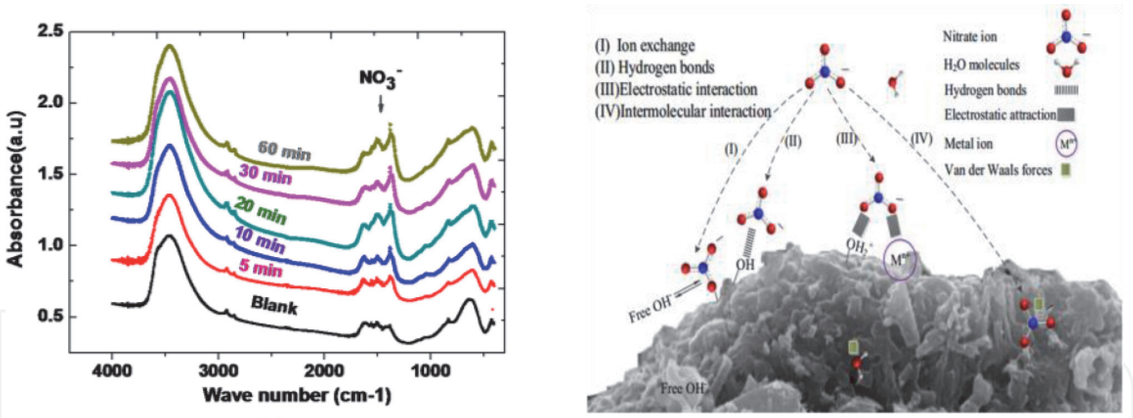

Figure 2.
(a) FT-IR spectra of Zn_3-Al-Cl visualized and (b) proposed adsorption mechanism between the adsorbent and nitrate [22].

Sample	Ratio	υ (OH) (cm^{-1})	δ (H_2)) (cm^{-1})	ν (M O) (cm^{-1})	δ (O M O) (cm^{-1})
Zn_3-Al-Cl-LDH-blank	R = 3	3454.6	1628	613.38	426.28

Table 1.
Frequencies of absorbance bands.

3.3 Inductively coupled plasma (ICP) spectrometry

The chemical formula Zn_3-Al-Cl-LDH was obtained using the technical ICP analysis, which shows that the theoretical ratio [R = (Zn^{2+}/Al^{3+})] is close to that of the synthesis. This characterization also suggests that the sample has a homogeneous chemical composition; the approximate chemical formula is ($Zn_{2.93}Al(OH)_{7.86}$) (Cl^{-}. 1.87 H_2O) for the metal ratio of R = 3. Cl^{-} anion intercalated.

3.4 Study of the adsorption in batch and determination of nitrate ions

3.4.1 Calibration curve

A series of vials of 50 ml each containing 1 mL of 0.5% sodium salicylate is introduced: 8, 6, 4, and 2 ml of KNO_3 solution (50 mg L^{-1}) with, respectively, 2, 4, 6, and 8 ml of water. The contents of each flask are then evaporated to dryness in an oven (75–80°C) to produce a residue which is dissolved with 2 ml of concentrated H_2SO_4. After 10 min of rest has passed, 15 ml of distilled water and then 15 ml of a basic solution made up of 40% NaOH, 6% sodium potassium tartrate, and then 50 ml with distilled water are then allowed to develop the yellow color characteristic of the complex nitrate formed. The nitrate ion concentrations in the liquid phase were determined by a spectrophotometric method (spectrophotometer type JASCOV-630 λ = 415 nm).

The calibration curve obtained (**Figure 3**) is in good agreement with the Beer-Lambert law.

3.4.2 Assays of nitrate ions in balance

The Zn_3Al-Cl-LDH is contacted with a potassium nitrate solution (0.4 g/L) for 5 min, 10 min, 20 min, 30 min, and 60 min. Before washing Zn_3Al-Cl-LDH after

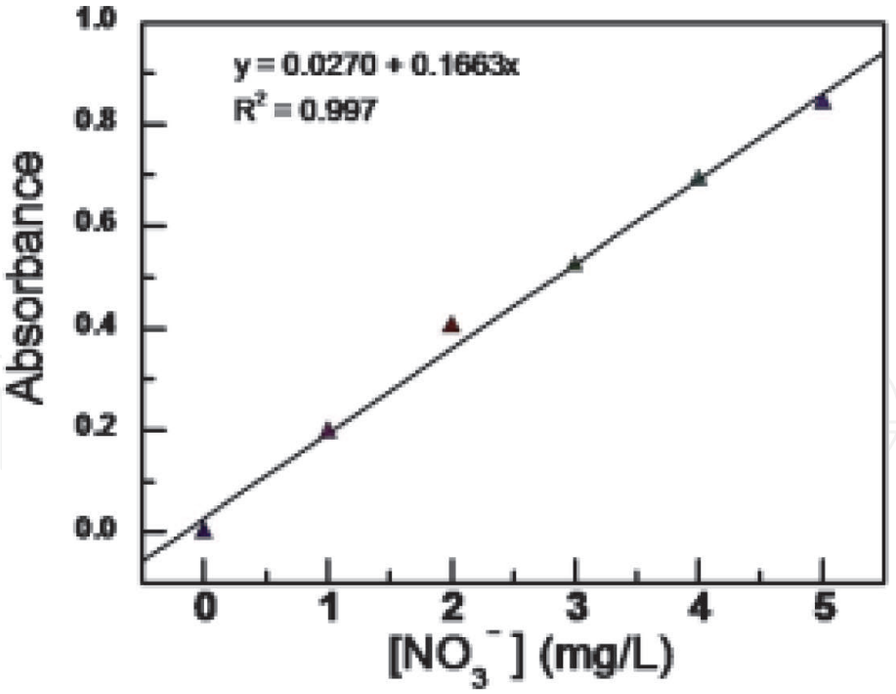

Figure 3.
Curve calibration of spectrophotometer used for determination of NO_3^- adsorbed.

adsorption and which is intended for the dielectric analysis. The filtrate is recovered corresponding to each time and fee in 1 mL is put in a 50 mL flask and then the following procedure used for the tracing of the calibration curve.

3.5 Kinetic study

The adsorption kinetic studies were carried out by contacting Zn_3Al-Cl-LDH (C_m = 0.8 g/L) with NO_3^- solutions (500 ml) of the initial concentration of 0.4 mg/L, respectively. The adsorption process was agitated at 25°C and a pH of 7.0 for several periods ranging from 5 to 60 min under inert atmosphere (N_2). LDH obtained after adsorption was filtered and then washed several times. The concentration of the nitrate ion in the filtrate was determined by spectrophotometer at 415 nm. The nitrate amount q_e (mg/g) loaded on adsorbents after adsorption experiments and the percentage removal (removal %) of NO_3^- ions from solutions were calculated using the following equations:

$$q_e = \frac{(C - Ce) \times V}{m} \tag{1}$$

and the removal

$$(\%) = \frac{C_0 - C_e}{C_0} \times 100 \tag{2}$$

where Ce (mg/L) is the equilibrium of nitrate ion concentration in solution, C_0 (mg/L) is the initial of nitrate ion concentration in solution, m (g) is the mass of adsorbent, and V (L) is the volume of the solutions.

The equilibrium is reached after 30 min, with a maximum of approximately 59.12% adsorption capacity corresponding to a 295.62 mg/g of an affinity of the adsorbate for the active sites of the adsorbent [23]. From **Figure 3** it is quite clear that the percentage of nitrate ion adsorption calculated by kinetic study and

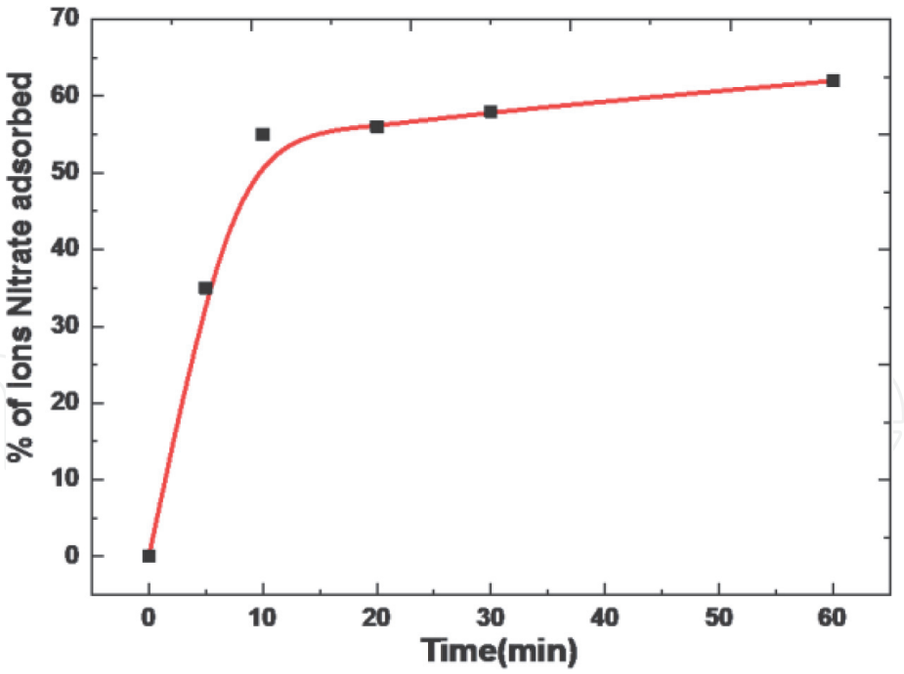

Figure 4.
Kinetic study evaluation of NO_3^- removal by Zn_3AlCl-$(NO_3^-)_{ads}$ complex.

efficiency adsorption calculated by impedance spectroscopy are less than 10% which shows that the values are close and both techniques are okay and best correlated. From **Figure 4** adsorption of nitrate ions by this system noted as a function of adsorption time is quite rich on information. The adsorption phenomena are due to the active sites in LDH interlayer with different electron donor sites (active adsorption sites) on the ions (N&O) and relative humidity [24–26].

3.6 Analysis of adsorption kinetics

The different kinetic models including pseudo-first-order, pseudo-second-order, and intraparticle diffusion are employed to investigate the mechanism of adsorption and potential rate controlling steps such as chemical reaction mass transport and diffusion control processes [27]. The pseudo-first-order and pseudo-second-order are generally expressed as Eqs. (3) and (4), respectively (**Figure 5**):

$$\mathrm{Log}\left(q_e - q_t\right) = \mathrm{Log}\left(q_e\right) - \frac{K_{1,ads}}{2,303} \times t \tag{3}$$

$$\frac{t}{q_t} = \frac{1}{K_{2,ads} \times q_e^2} + \frac{t}{q_e} \tag{4}$$

where qe (mg/g) and q_t (mg/g) are the adsorption of NO_3^- ions on to adsorbents at equilibrium and at time t (min), respectively; $K_{1,ads}$ (min^{-1}) and $K_{2,ads}$ (g/(mg min)) are the constants of the pseudo-first-order and pseudo-second-order adsorption, respectively. Additionally h (mg/(g min)) is the initial adsorption rate of pseudo-second-order which can be calculated using h = K_2qe2.

The adsorption rate constants $k_{1,ads}$ and $k_{2,ads}$ of nitrate ions by (Zn_3Al-Cl-LDH) are deducted, respectively, from the curve $\log(q_e\text{-}q) = f(t)$ and $(t/q_t) = f(t/q_e)$ (**Figures 6** and 7).

The regression by the pseudo-second-order model agrees well to study the adsorption of the nitrate ions by Zn_3Al-Cl-LDH. The constant of adsorption rate

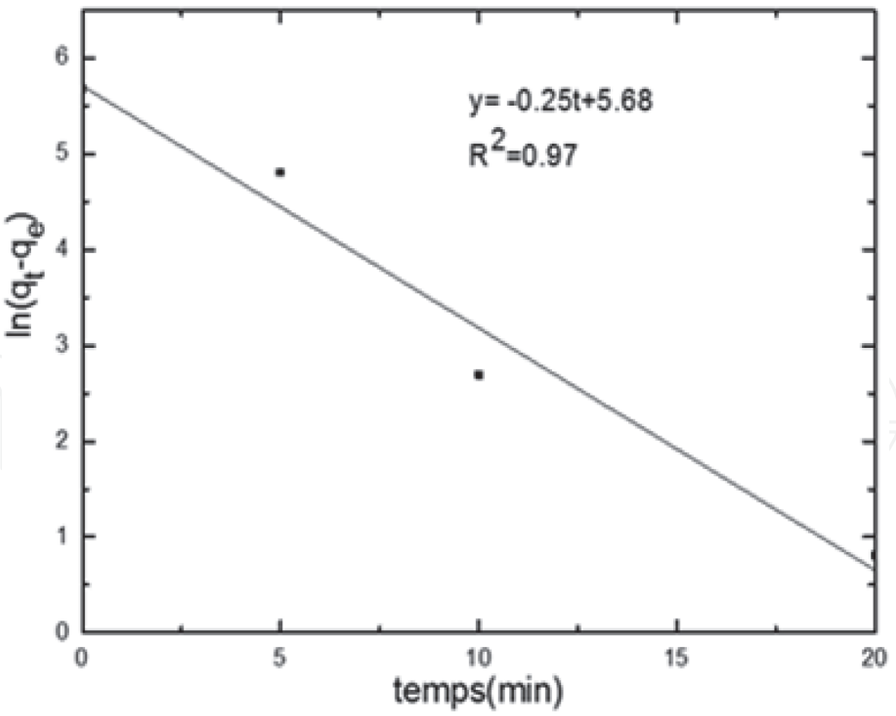

Figure 5.
Pseudo-first-order model removal NO_3^- by (Zn_3Al-Cl-LDH).

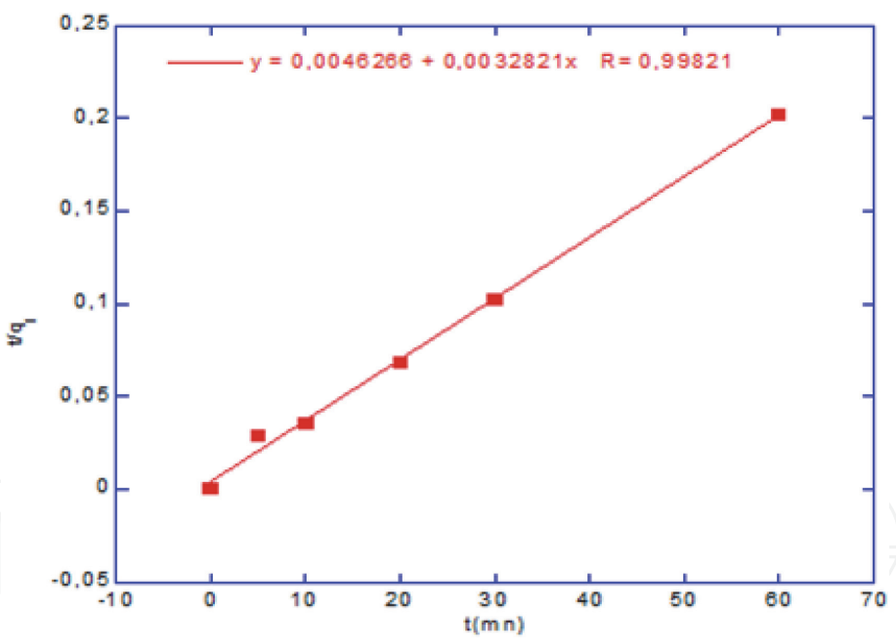

Figure 6.
Pseudo-second-order model of removal NO_3^- by Zn_3-Al-Cl-LDH.

confirms the rapid process noted during the kinetic study. The maximum amount obtained by applying the pseudo-second-order model is very close to that determined by the kinetic study (~296 mg/g).

The values of the correlation factors obtained (**Table 2**) show that the measurement data of kinetics follows the pseudo-second-order model ($R^2 \approx 0.99$).

3.7 Constant diffusion rate determination

Intraparticle diffusion equation suggests that intraparticle diffusion is the rate-limiting step in adsorption. The diffusion process may affect the adsorption of

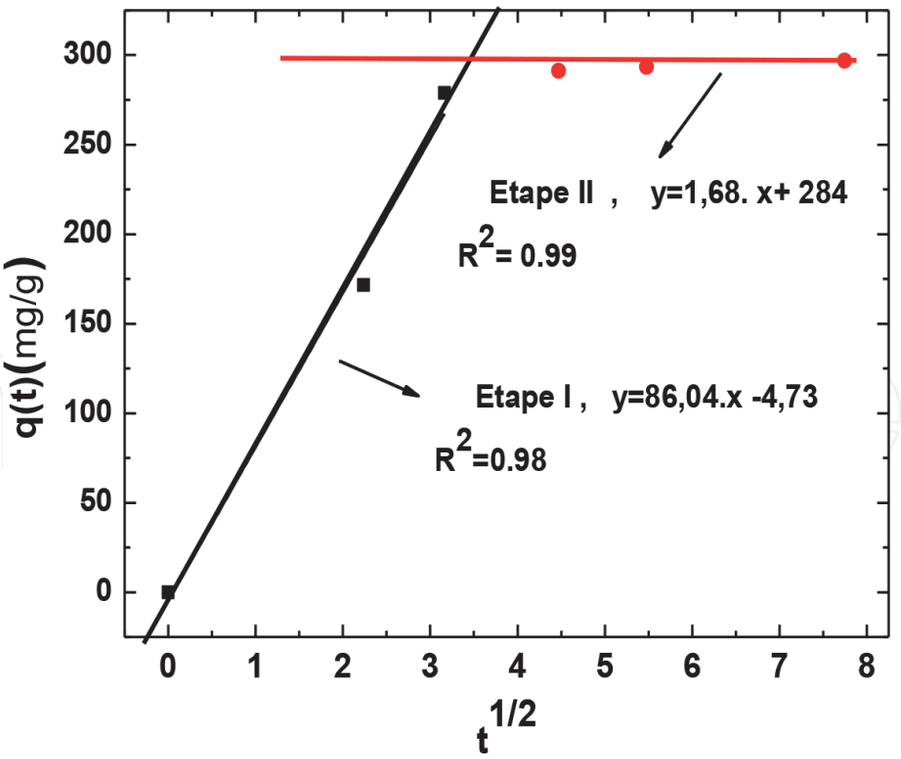

Figure 7.
Intraparticle diffusion model for Zn_3Al-Cl-$(NO_3^-)_{ads}$-LDH complex.

Pseudo-first-order			Pseudo-second-order		
$K_{1.ads}$ (min^{-1})	qe (mg/g)	R^2	$K_{2.ads}$ (g/mg/min)	qe (mg/g)	R^2
0.25	292.94	0.94	0.002	312.5	0.99

Table 2.
Kinetic parameters for Zn_3Al-Cl-$(NO_3^-)_{ads}$-LDH complex.

nitrate ions on Zn_3-Al-Cl-LDH due to the porous structure of the adsorbent and the attractive effect of nitrate ions. Therefore the intraparticle diffusion is used to explore the behavior of intraparticle diffusion is obeys Eq. (5) [27].

$$q_t = kip.t^{1/2} + C \quad (5)$$

where qt is the quantity retained at time t and kip are the diffusion rate constants.

The results obtained (**Figure 6**) show that there are two stages. *Region 1* is attributed to the most readily available site on the surface of the adsorbent. *Region 2* can be explained by a very slow diffusion of adsorption in the inner pores. Thus the nitrate ion adsorption by Zn_3-Al-Cl-LDH may be governed by the intraparticle model [1]. The values of kp1 and kp2 diffusion rate constants for Region 1 and Region 2, respectively, obtained by using the regression linear are shown in **Table 2**.

These values are in good agreement with the kinetic study. Indeed, in Region 1 the value of the slope (86.04) is greater than that of the Region 2 whose value is of the order of 1.68. This can be explained by the availability of sites in Zn_3-Al-Cl-LDH at the beginning of adsorption. The release rate constants intraparticle using the kinetics study was according the values respectively K_{1P} = 86.04 with the R^2 = 0.98 and K_{2P} = 1.68 with the R^2 = 0.99. The adsorption of nitrate ions by Zn_3-Al-Cl-LDH is confirmed by FT-IR spectroscopy. In fact the infrared spectra of the materials

recovered after adsorption at various times (**Figure 6**) show the increase of the intensity of the characteristic band of NO_3^- at 1381 cm^{-1} in a function of contact time of ions.

It could be seen that the plots were multilinear over the whole time range suggesting that two steps were operational in the adsorption of NO_3^- by Zn_3-Al-Cl-LDH. The first linear plot was the instantaneous adsorption or external surface adsorption attributing to the rapid consumption of the available adsorption sites on the adsorbent surface. The second stage was the gradual adsorption stage where the intraparticle was the rate-limiting step, and the second portion was attributed to the final equilibrium for which the intraparticle diffusion starts to slow down due to the extremely few adsorption sites left on adsorbent which will be clearly in impedance spectroscopy using the Nyquist diagram analysis by means of fit and extrapolation of experimental data for both adsorption regions.

4. Impedance spectroscopy analysis

Using impedance spectroscopy one can distinguish between intrinsic (grain) and extrinsic (grain boundaries). The Nyquist and Bode plots were used to interpret the electrical relaxation processes associated with adsorption phenomenon and used to search for the electrical analogue of the adsorption.

In order to determine the mechanisms responsible for the conductivity, in general, the different variations of complex impedance spectra (Nyquist plot) consist of two semicircle arcs corresponding to the grain interior and grain boundary. The arc at a high frequency usually represents the grain response, and the low-frequency arc corresponds to the grain boundary [28].

The impedance analysis allows one to determine the contributions of various processes such as bulk effects and the grain boundaries. **Figure 8** shows the complex impedance plane plots (Nyquist plot) of the nitrate ion removal by the system Zn_3-Al-Cl-LDH (0 min ≤ t ≤ 60 min).

The analysis (**Figure 8a** and **b**) of the data by the Nyquist diagram allowed us to determine the resistance values for the two regions in the time interval of 0, 5, and 10 min (Region 1) and 20, 30, and 60 min (Region 2). The separation into two time intervals is justified by **Figure 7** of the kinetic study and **Figures 9** and **10** of the impedance spectroscopy study.

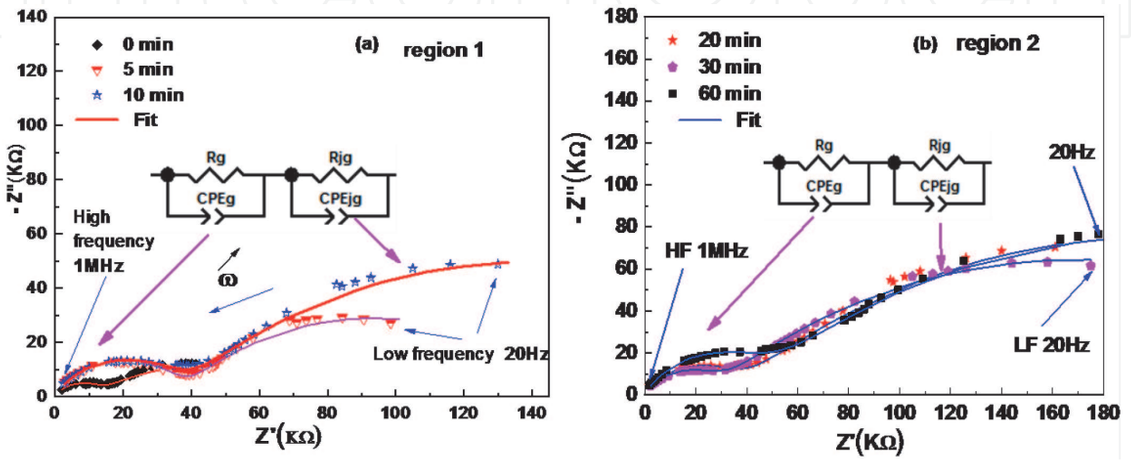

Figure 8.
Nyquist plots for samples in Region 1 (a) and Region 2 (b), respectively, during adsorption phenomenon by Zn_3Al-Cl-$(NO_3^-)_{ads}$-LDH.

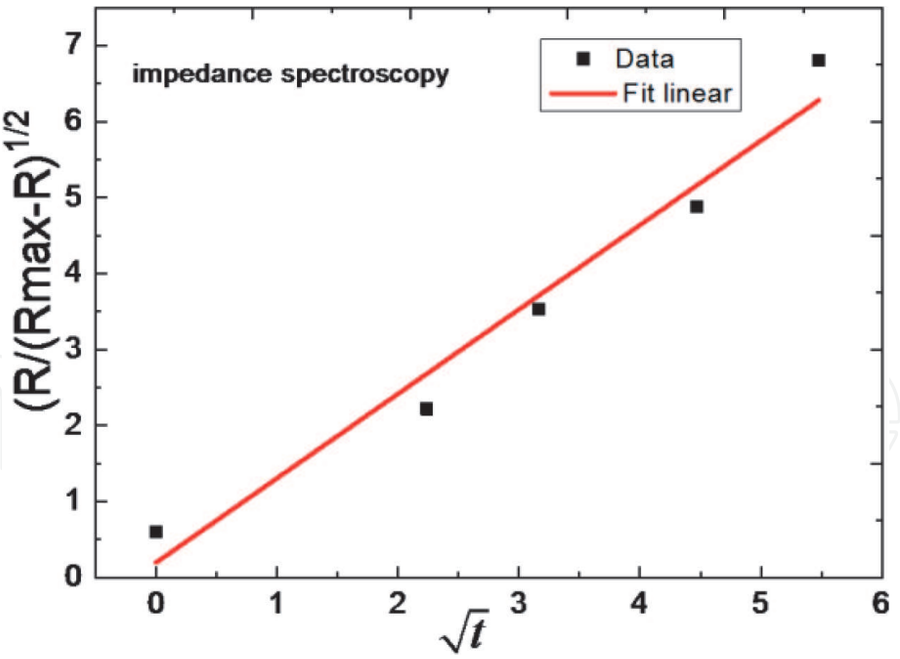

Figure 9.
Variation of the ratio (R_{bg}/R_{bgmax}-R_{bg}) according to the square root of the adsorption time.

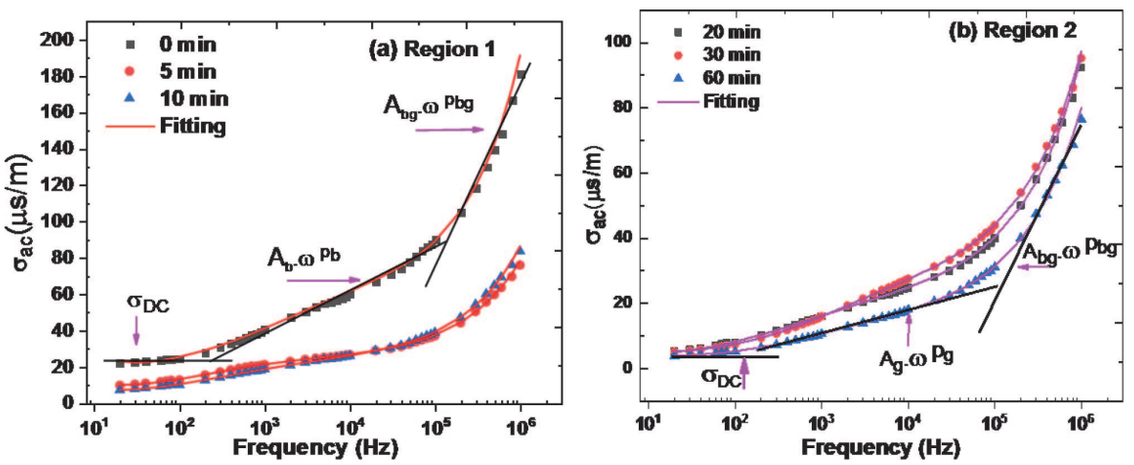

Figure 10.
Variation of σ'ac conductivity for (a) Region 1 and (b) Region 2 as a function of frequency.

Figure 11 shown is intended to show that there are only two capacitive loops in the extrapolation technique of experimental data in a frequency range of 10^{-2} Hz to 1 MHz: one for the contribution of grain region and the other for grain boundary contribution.

The estimated value of R is the difference between the high intercept and low intercept values. If the data reflects a parallel R-C element with a depression angle of zero, the estimated R will be the same as the diameter of the semicircle. Estimated C is calculated using the relationship $\omega_{max} = 1/(RC)$ and depends on the accuracy of ω_{max}.

The Nyquist (**Figures 12** and **13**) plot studies discovered the presence of grain and grain boundary which then become dipoles when they are subjected to the action of an electric field. We thus observe two phenomena of relaxations, no more of which are observed as the maximum in the Nyquist plot (Cole-Cole). We also find that we have two different regions that are two constants of the time τ_g and τ_{bg} using extrapolation by a corresponding equivalent circuit of data, which leads us to say this kinetic is mixed and it is what we confirmed by the chemical kinetic study.

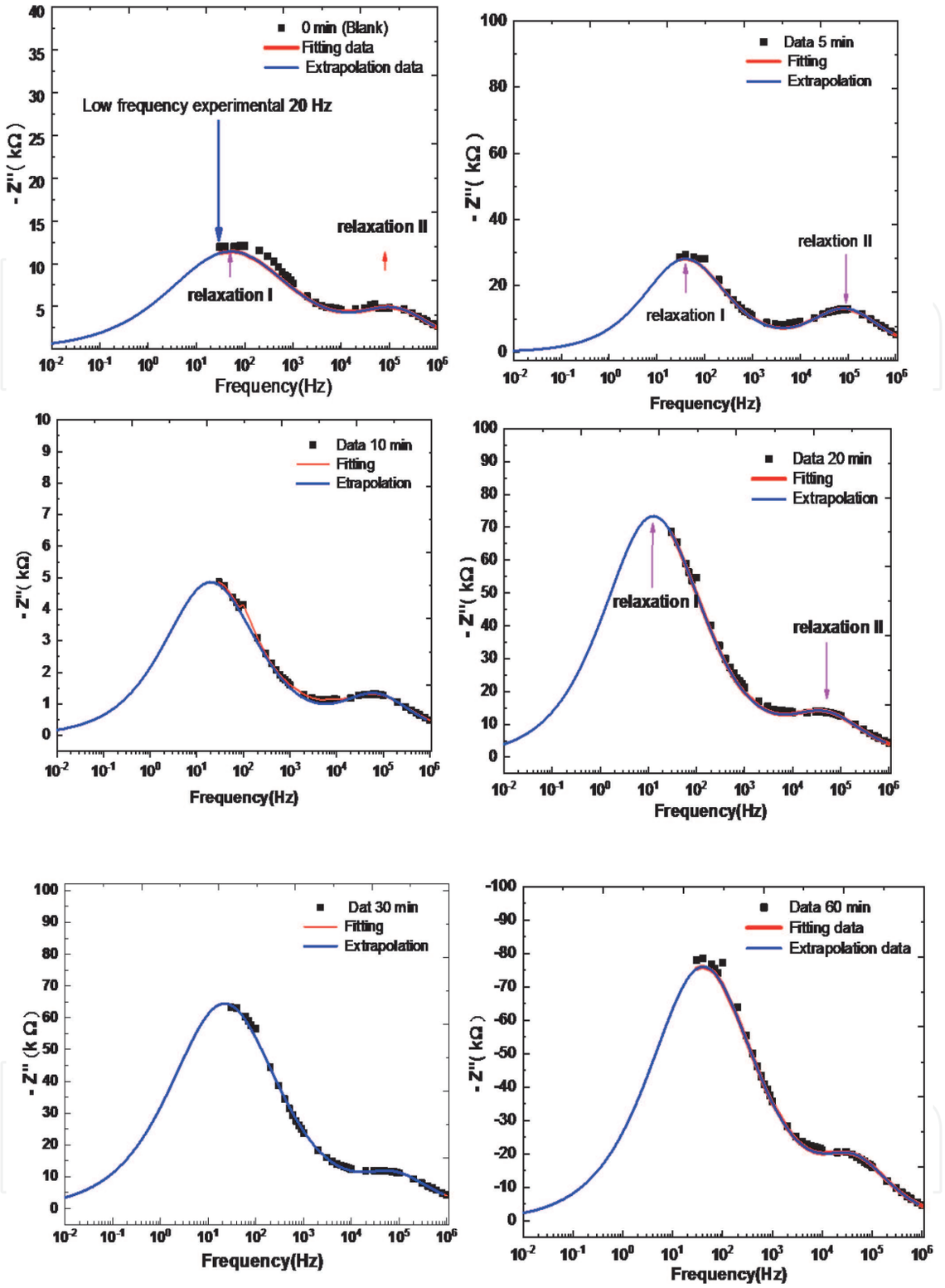

Figure 11.
Superposition of experimental data done by the equivalent electrical circuit and extrapolation of different adsorption times.

After analyzing and evaluating the spectra using ZView 2.2 software, we extracted the parameters mentioned in **Table 3**. From the values shown in **Table 3**, it is observed that the adsorption efficiency increases when showing the fixing of nitrate ions on the surface of Zn_3-Al-Cl-LDH. We used other quantities extracted from the equivalent circuit. The quantities are the dispersion coefficient for the grain and the grain boundary, on the one hand, and the grain and grain seal capacity, on the other hand, as a function of the adsorption time in order to follow

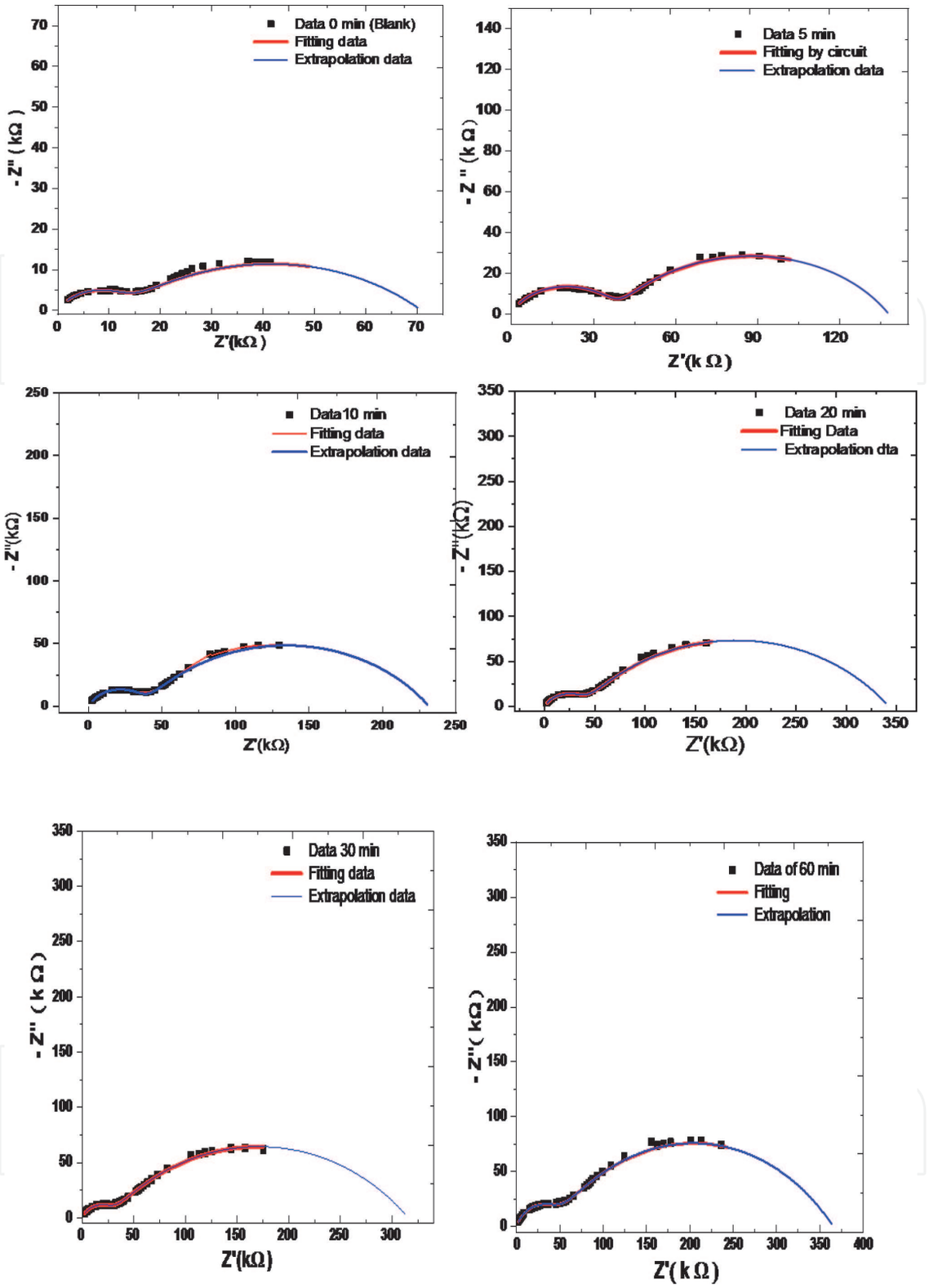

Figure 12.
Fitting and extrapolation of data experimental using equivalent circuit at all times of adsorption at room temperature.

the phenomenon of adsorption of the nitrate ions to the available pores of Zn_3-Al-Cl-LDH.

4.1 Intraparticle diffusion rate constant

In order to test the existence of intraparticle diffusion in the adsorption process, the amount of nitrate adsorbed per unit mass of adsorbents q at any time t was

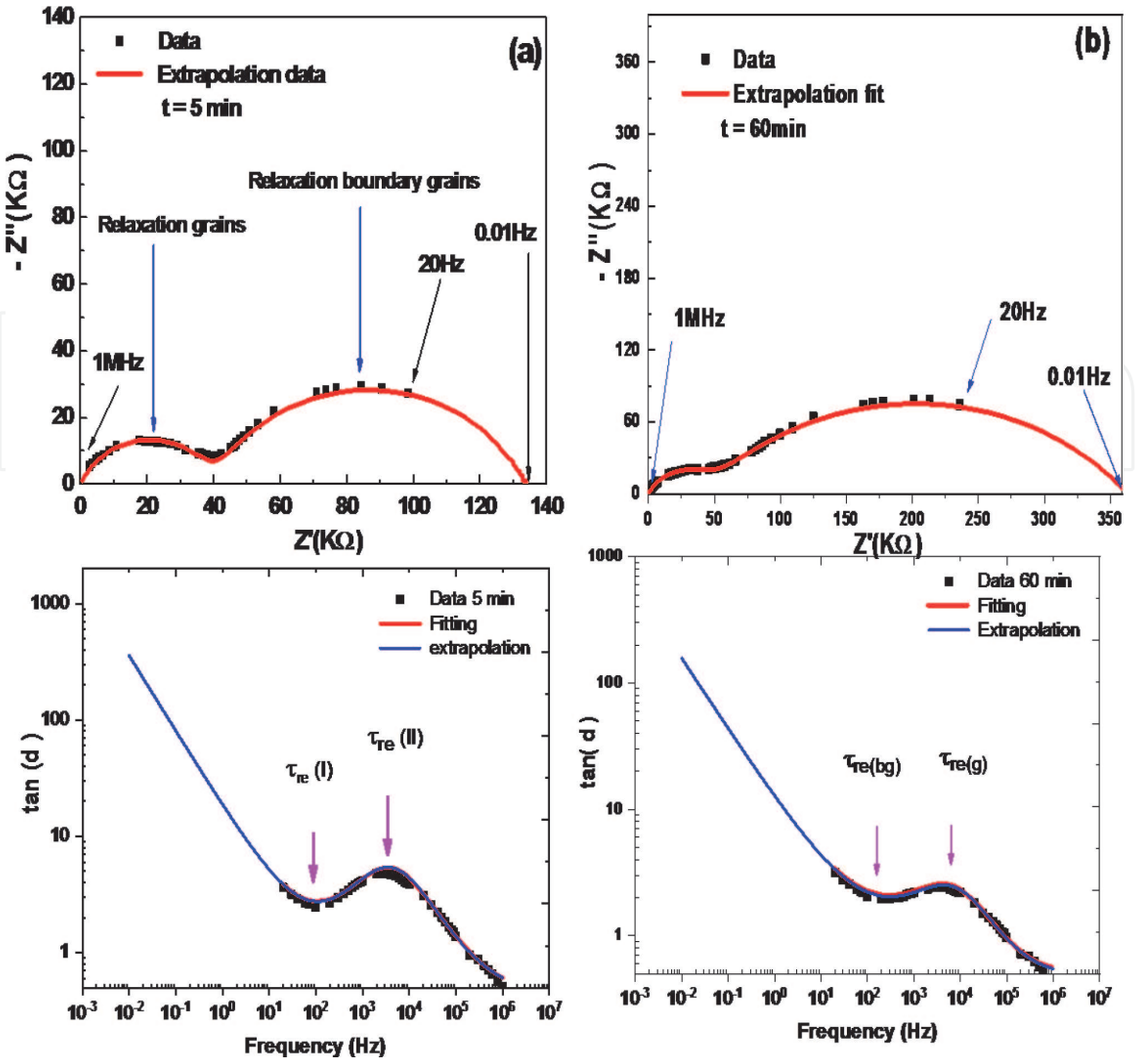

Figure 13.
Extrapolation of tan (d) measurement data of Zn_3-Al-Cl-LDH for t = 5 min (a) and (b) t = 60 min.

Sample	Rg (Ω)	(E%)g	R_{bg} (Ω)	$(E\%)_{bg}$	pg	p_{bg}	Tg ($\Omega^{-1.s\alpha}$)	T_{bg} ($\Omega^{-1.s\alpha}$)	X^2
0	11,513	0	61,702	0	0.71	0.43	2.05	1.42	0.003
5	36,160	2.14	157,410	1.55	0.73	0.63	1.90	0.34	0.001
10	40,275	2.49	196,670	2.19	0.74	0.62	1.64	0.23	0.001
20	41,753	2.62	302,160	3.90	0.75	0.63	1.49	0.28	0.001
30	42,584	2.69	298,590	3.84	0.76	0.64	1.43	0.24	0.0008
60	43,504	2.77	319,590	4.18	0.77	0.66	1.39	0.14	0.0001

Table 3.
The values of the fitted corresponding equivalent circuit parameters.

plotted as a function of square root of time ($t^{1/2}$). The rate constant for intraparticle diffusion was obtained using the Weber-Morris equation given as follows [35]:

$$q(t) = k_p.\sqrt{t} + c \tag{6}$$

where q is the amount of nitrate adsorbed in mg/g of adsorbent, k_p is the intraparticle diffusion rate constant, and "t" is the agitation time in minutes. Due to stirring, there is a possibility of transport of nitrate species from the bulk into the

pores of the LDH as well as adsorption at an outer surface of the LDH. The rate-limiting step may be either adsorption or intraparticle diffusion.

Different regions of a system sample are characterized using a resistance and a constant phase element (CPE) placed usually in parallel, where subindexes "g" and "gb" refer to grain and grain boundary, respectively (Eqs. 7 and 8):

$$\tau_g = \left(R_g.T_g\right)^{\frac{1}{p_g}} \quad \text{and} \quad \tau_{jg} = \left(R_{jg}.T_{jg}\right)^{\frac{1}{p_{jg}}} \tag{7}$$

$$C_g = R^{\frac{1}{pg}-1}.T^{\frac{1}{pg}} \quad \text{and} \quad C_{jg} = R^{\frac{1}{pjg}-1}.T^{\frac{1}{pjg}} \tag{8}$$

The values of the individual $R_g.C_g$ and $R_{bg}.C_{bg}$ components may then be quantified. Let us now see some practical examples of data and interpretation. A common type of impedance spectrum for Zn_3-Al-Cl-$(NO_3^-)_{ads}$ LDH shows the presence of two distinct features attributable to intergrain or bulk and intergrain or grain boundary regions, using Eqs. (7) and (8) for obtained correspondent values listed in **Table 4**.

4.2 AC conductivity analysis

The ionic conductivities extracted from the data using the equivalent circuit of **Figure 14** depicted in **Figure 15a** and **b** show the variation of AC conductivity with frequency at various times of adsorption for nitrate ions in the surface of the ionic clay. The log–log curves are flat in the low-frequency region as the conductivity values approach those of the DC conductivity. As frequency increases, the curves become dispersive. In the high-frequency range, weak time dependence may be noted, and it is evident that the shapes of the curves are similar. In most materials AC conductivity due to localized states may be described using the equation of double power law of Jonscher [29]. In the electrical conductivity at different times of adsorption, it is clear from the plot that above a certain point, the conductivity increases linearly with frequency. From **Figure 8**, it is also evident that the DC contribution is important at low frequencies and the high time of adsorption, whereas the frequency-dependent term dominates at high frequencies [30–34].

It can be observed (**Figure 15a** and **b**) that increased with increasing frequency. This can be explained in terms of conductivity of grains separated by highly resistive grain boundaries. According to this model, the AC conductivity at low frequencies exhibited the grain boundary behavior, while the dispersion at high frequency is attributed to the conductivity of grains. This variation corresponding to the interpretation of LDH materials has two types of charge carrier, which are responsible for the dielectric relaxation [35]. As reported in our earlier article [36], the proton of the polarized clusters of water is the first carrier, and the nitrate ions

Time (min)	τ_g (ns)	τ_{jg} (μs)	C_g (pF)	C_{jg} (nF)	R_{jg}/C_{jg}	K_p
0	1.10	3.91	0.95	0.63	0.13	0.00
5	2.00	5.35	0.51	0.49	0.29	0.62
10	2.60	10.9	0.64	0.55	0.47	0.83
20	2.90	19.95	0.79	0.66	0.60	0.92
30	3.06	17.13	0.69	0.57	0.69	0.96
60	3.36	9.03	0.77	0.28	0.95	1.00

Table 4.
Results obtained by the corresponding equivalent electrical circuit.

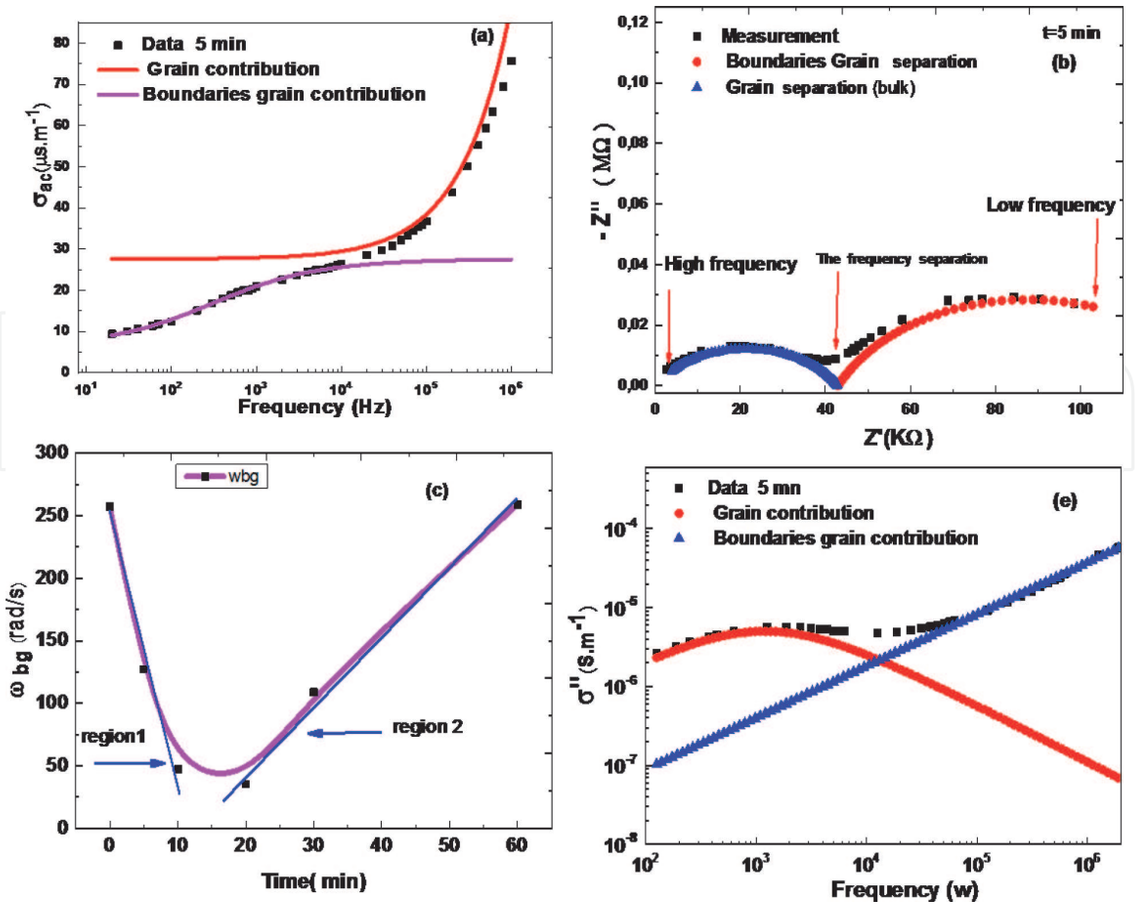

Figure 14.
Separation behavior of the conductivity (a) of grains and grain boundaries. (b) Nyquist diagram showing the behavior of the grain and grain boundary for the adsorption time 5 min. (e) and (e) in the representation of the imaginary part of the conductivity. (c) Variation of the grain boundary pulsation for the adsorption time 5 min.

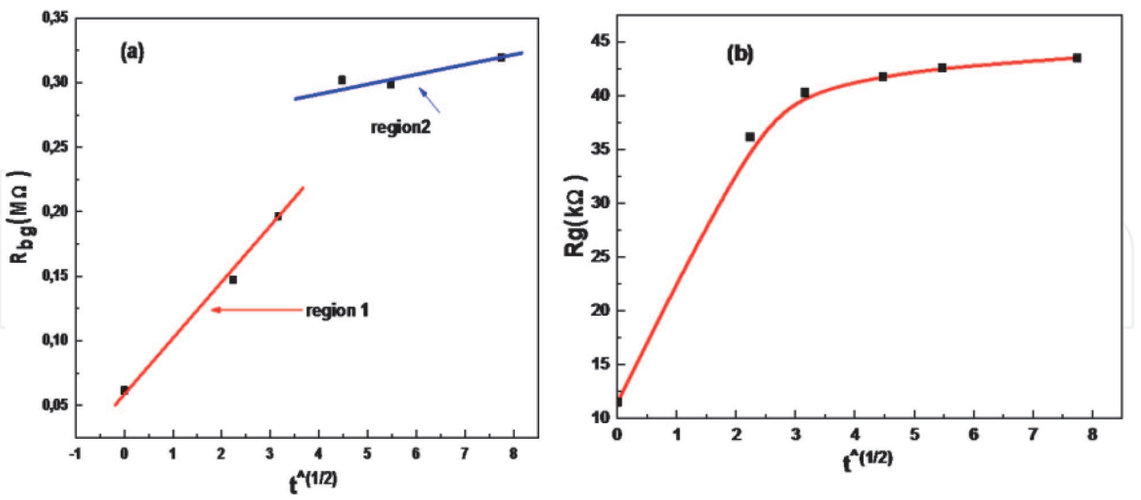

Figure 15.
Variation of the resistor (a) grain boundaries and (b) grains as a function of square root of time.

of the adsorption surface of LDH region (**Figure 2b**) is the second one. The proton transfers to produce OH^- and HO_3^+ ions (hydrogen bonding) at every path end of water clusters in the presence of the applied electric field due to proton hopping (inter-cluster hopping at low-frequency region and intra-cluster hopping at high frequency) (**Figure 2c**). In this condition, nitrate ions also transfer from their equilibrium positions to serve as an additional charge carrier.

Figures 13 and **15** show that σ'ac (ω) becomes almost independent of frequency below a certain value when it decreases with decreasing frequency. The ionic σ'ac (ω) conductivity will be obtained using the technical extrapolation of this part of spectra toward lower frequency.

The conductivity σ'ac frequency dependence can be described in the majority of ionic conductors by the simple power law Jonscher according to [37] descript be one term dispersion although our system provides else dispersion term depicted in **Figures 7** and **8**.

$$\sigma'_{ac}(\omega) = \sigma_{DC} + A_g\omega^{p_g} + A_{bg}\omega^{p_{bg}} \tag{9}$$

The charge carriers are the adsorbed nitrate ions, and the protons originate from adsorbed mobile water located on the surface of the clay [4]. On the other hand the charge carriers are responsible for the second jump which is generated by the anions Cl^- and the H_3O^+ ions intercalated in the interlamellar region according to [38].

The slope changes in the conductivity variation depicted in **Figure 10a** and **b** confirms that the conductivity of our system exhibits two behaviors of frequency dispersion: low-frequency dispersion associated with grains and the other for grain boundaries (**Figure 14a** and **b**).

Usefulness of figures: **Figure 10a** of variation suggests the presence of a hopping mechanism in these samples. Such type of conducting behavior is well described by Jonscher's universal power law. On the other hand, our system presents two power laws.

The **Figure 10b** of variation suggests two contributions grains and boundaries grains. This manifest itself in the conductivity diagram, with two hopping conductions which lead to two different slopes.

The figure shows that the joint region of grains is the regions that adsorb nitrate ions, but this variation influences the grain region. On the other hand, this finding is in good agreement with the evolution shown in **Figure 16a**.

The figure presents the deconvolution in order to separate contributions grains and grain boundaries as a function of frequency.

4.3 Modeling of the electrical conductivity through the equivalent electrical circuit

From the modeling performed by an electrical circuit during the study of intercalation according to [39, 40], we have learned some physical characteristics of this

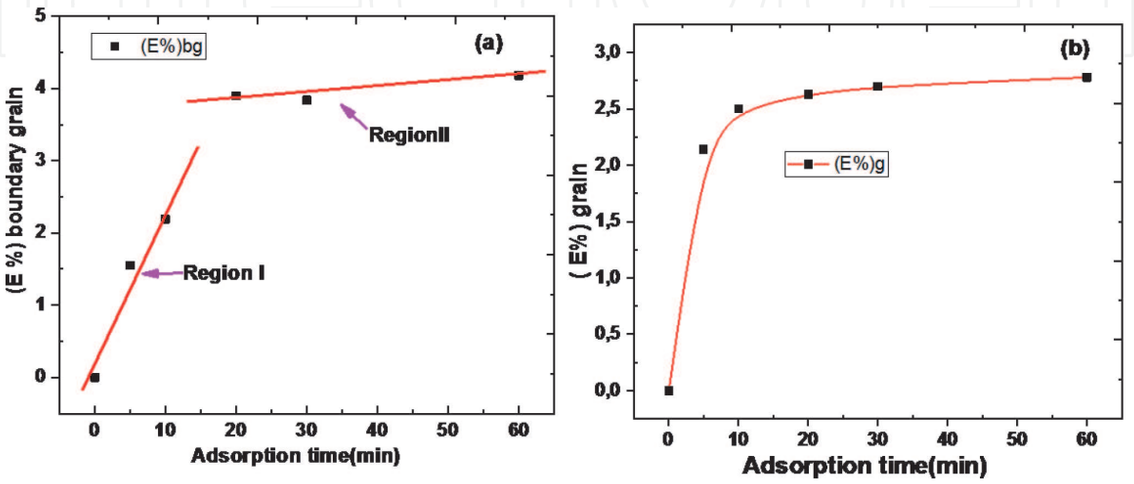

Figure 16.
Variation of the percentage of the relative difference in (a) grain boundary resistance and (b) grain at the different times of adsorption.

material. The circuit consists of a resistor in parallel with a constant phase element (CPE) characterized by a pseudocapacitance and Tp (scattering coefficient).

The conductivity of this circuit is of the following form [40]:

$$\sigma'_{ac}(\omega) = \frac{e}{S} \times y'(\omega) \tag{10}$$

where the real part of the admittance is

$$Y'(\omega) = \frac{1}{R}\left(1 + (\omega\tau)^{p} \cos\left(\frac{p\pi}{2}\right)\right) \tag{11}$$

Using the simulation of Eq. 11, we have obtained the equation of the admittance of grain established by the following expression:

$$Y'_{g}(\omega) = \frac{1}{R}\left[1 + (\omega\tau)_{g}^{p_g} \cos\left(\frac{p_g\pi}{2}\right)\right] \tag{12}$$

Finally the conductivity of grain is shown in the following equation:

$$\begin{aligned}
\sigma'_{ac}(\omega) &= \frac{k}{R}\left[1 + (\omega\tau)_{g}^{pg} \cos\left(\frac{pg\pi}{2}\right)\right] = \sigma_{dcg} + \frac{k}{R} \times (\omega\tau)_{g}^{pg} \cos\left(\frac{p_g\pi}{2}\right) \\
\sigma'_{ac}(\omega) &= \sigma_{dcg}\left(1 + (\tau)_{g}^{p_g} \cos\left(\frac{p_g\pi}{2}\right) \times \omega^{p_g}\right) \\
\sigma'_{ac}(\omega) &= \sigma_{dcg}\left(1 + \left(\frac{\omega}{\omega_{hg}}\right)^{pg}\right)
\end{aligned} \tag{13}$$

with $\omega_{hg} = \left\{\tau_{g}^{pg} \cos\left(\frac{pg\pi}{2}\right)\right\}^{-1}$ the pulsation of hopping

In the term of conductivity, plots of the lower frequency dispersion correspond to the presence in grain boundary; this region can be approximately modeled by the circuit similar to the one depicted in **Figure 17** (grain boundary).

By similar calculations, the expression of the grain seal conductivity follows the shape of the following expression:

$$\begin{aligned}
\left(\sigma'_{ac}(\omega)\right)_{bg} &= \frac{k}{R} \times \left[1 + (\omega\tau)_{bg}^{p_{bg}} \times \cos\left(\frac{pbg\pi}{2}\right)\right] \\
&= (\sigma_{dc})_{\mathrm{bg}} + \frac{k}{R} \times (\omega\tau)^{p_{gb}} \cos\left(\frac{p_{bg}\pi}{2}\right) \\
\left(\sigma'_{ac}(\omega)\right)_{\mathrm{bg}} &= (\sigma_{dc})_{\mathrm{bg}} \times \left[1 + (\tau)_{bg}^{p_{bg}} \cos\left(\frac{p_{bg}\pi}{2}\right)\right] \times \omega^{p_{bg}}, \\
\left(\sigma'_{ac}(\omega)\right)_{\mathrm{bg}} &= (\sigma_{dc})_{\mathrm{bg}} \times \left[1 + \left(\frac{\omega}{\omega_{hbg}}\right)^{p_{bg}}\right]
\end{aligned} \tag{14}$$

with $\omega_{h_{bg}} = \left\{\tau_{bg}^{p_{bg}} \cos\left(\frac{p_{bg}\pi}{2}\right)\right\}^{-1}$ is the pulsation of hopping

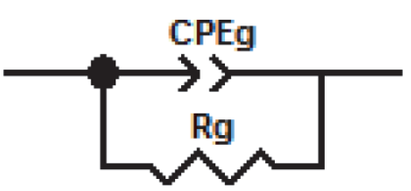

Figure 17.
Corresponding equivalent circuit used to fit by EIS experimental data of intercalation.

The total conductivity of the sample is similar for the different adsorption times; the evolution is typical called the double power law of Jonscher [41].

From the modeling performed by an electrical circuit during the adsorption study, we learned some physical characteristics of this material through the equivalent circuit modeling of the grain boundaries according to literature reviews [42] (**Figure 18**).

Figure 19 shows the electrical conductivity of the sample as a function of frequency. Two different regions can be distinguished. In Region 1, the conductivity is dominated by grains and in Region 2 is dominated by boundary grains [42], where the conductivity increases with increasing frequency. The electrical conduction of the sample follows a consecutive hopping mechanism. Whenever it is transferred to another site, the surrounding molecules respond to this perturbation with structural changes, and the electron or hole is temporarily trapped in the potential well leading to polarization. Another aspect of this charge hopping mechanism is that the electron or hole tends to associate with local defects [3, 43].

The dependence of the AC conductivity on frequency can be expressed by the following law:

$$\sigma'_{ac}(\omega) = \sigma_{DC} + A_g \times \omega^{p_g} + A_{bg} \times \omega^{p_{bg}} \tag{15}$$

where Ag is a pre-exponential factor and Abg is the frequency exponent [8, 44–46], which generally is less than or equal to 1. **Figures 7** and **8** show the frequency dependence of the AC electrical conductivity at different times of adsorption. It is clear from the plot that above a certain point, the conductivity increases linearly with frequency. In these figures it is also evident that the DC contribution is important at small frequencies and high frequencies, whereas the frequency-dependent term dominates at high frequencies. Also in the low-frequency region, the conductivity depends on the time of adsorption. Such dependence may be described by the variable range hopping (VRH) mechanism also called hopping conduction mechanism. The value of A_g and A_{bg} in Eq. (13) was extracted from the slope of the plot of Log(σ'ac) versus Log(f), and this value was used to explain the conduction mechanism in the sample. The capacitance adsorption is called double layer capacitance is the dependence of values was plotted, and it is seen that the frequency

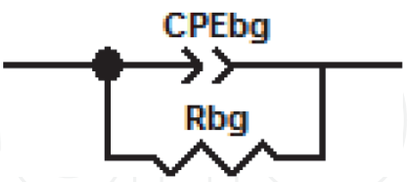

Figure 18.
Corresponding equivalent circuit to fit by EIS experimental data contribution of cluster ($NO_3^- H_3O^+$) adsorbed on the surface (grain boundary).

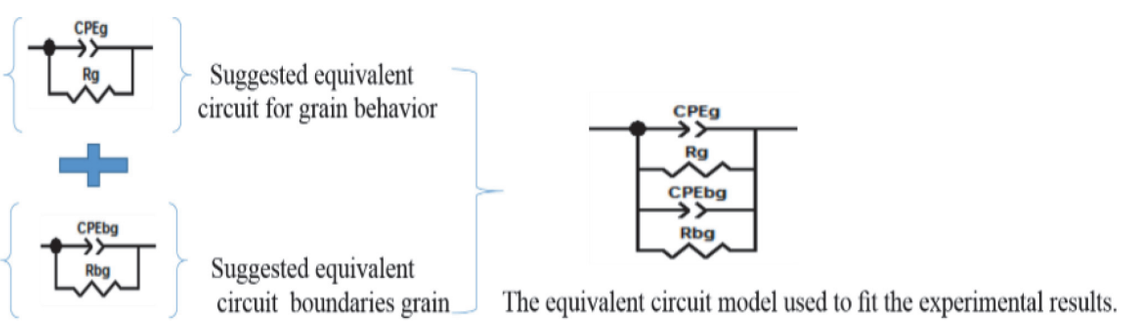

Figure 19.
Corresponding equivalent circuit used to fit the EIS experimental data of conductivity for sample study.

exponent decreases with increasing surface adsorption. This result is in clear agreement with the correlated barrier hopping (CBH) model, so the frequency dependence of σ'ac can be explained in terms of this model [47–53].

Better fundamental understanding of the adsorption phenomenon is modeled by the equivalent circuit depicted in parentheses (**Figure 19**).

This circuit has the expression of conductivity is following Eqs. 10. Use the fit by this circuit the results of the simulation are tabulated in **Table 5**. The values of the conductivity of grains and grain boundaries fitted and evaluated using the equivalent electrical circuit are reported in **Table 5**.

All frequency sweeps from this experiment were analyzed using the model of double power law to give σbg values σ_g grain relaxation time and grain boundary. In all cases the double power law provided an excellent fit to the data; **Figure 10a** and **b** is a plot of σ'_{dc} values as a function of frequency for the two regions.

In the model hopping, we distinguish two different characteristics in measurement frequency range. The charge transport takes place via an infinite percolation path in intermediate frequency. At high frequencies when the conductivity increases, the transport is dominated by a hopping contribution in finished areas of the system and is manifested in the variation of conductivity as a function of frequency by slope breaks such as p_g and p_{bg}.

4.4 Correlation between kinetic and impedance spectroscopy studies

Throughout in this study, the electrical properties of adsorption of nitrate by system LDH using the spectroscopy impedance as technical the investigation and monitoring of adsorption is important for the excellent result using the resistor of grains and the resistor of boundaries grains (**Figure 20**).

In order to attributed the second semicircle to a feature of the system, it is essential to have a picture of an idealized Zn_3Al-Cl-$(NO_3^-)_{ads}$-LDH with grains and grain boundaries and consider the factors which control the magnitude of the grain boundary impedance. **Figure 2b** model represents a Zn_3Al-Cl-$(NO_3^-)_{ads}$-LDH.

These results such as those shown in **Figure 21a-d** are useful for several reasons:

- To indicate whether the overall resistance of a material is dominated by bulk or grain boundary assured by the adsorption of nitrate
- To assess the quality and electrical homogeneity in the monitoring of adsorption since there is generally a link between sintering/microstructure and AC response.
- To measure the values of the resistances and capacitances at different times of adsorption

Time (min)	σ_g (μS/m)	σ_{bg} (μS/m)	τ_{bg} (μS)	τ_g (ms)	C_{bg} (nF)	C_g (pF)
0	8.685	1.620	1.10	3.89	1.01	0.634
5	2.770	0.7812	1.69	7.86	0.601	0.713
10	2.95	0.369	2.02	21.16	0.752	0.784
20	3.044	0.2493	2.58	28.26	0.983	0.704
30	3.761	0.34602	2.85	7.2	0.795	0.550
60	2.29	0.3125	3.35	3.86	0.895	0.121

Table 5.
Values of the conductivity relaxation time and the capacitance of grains and grain boundaries.

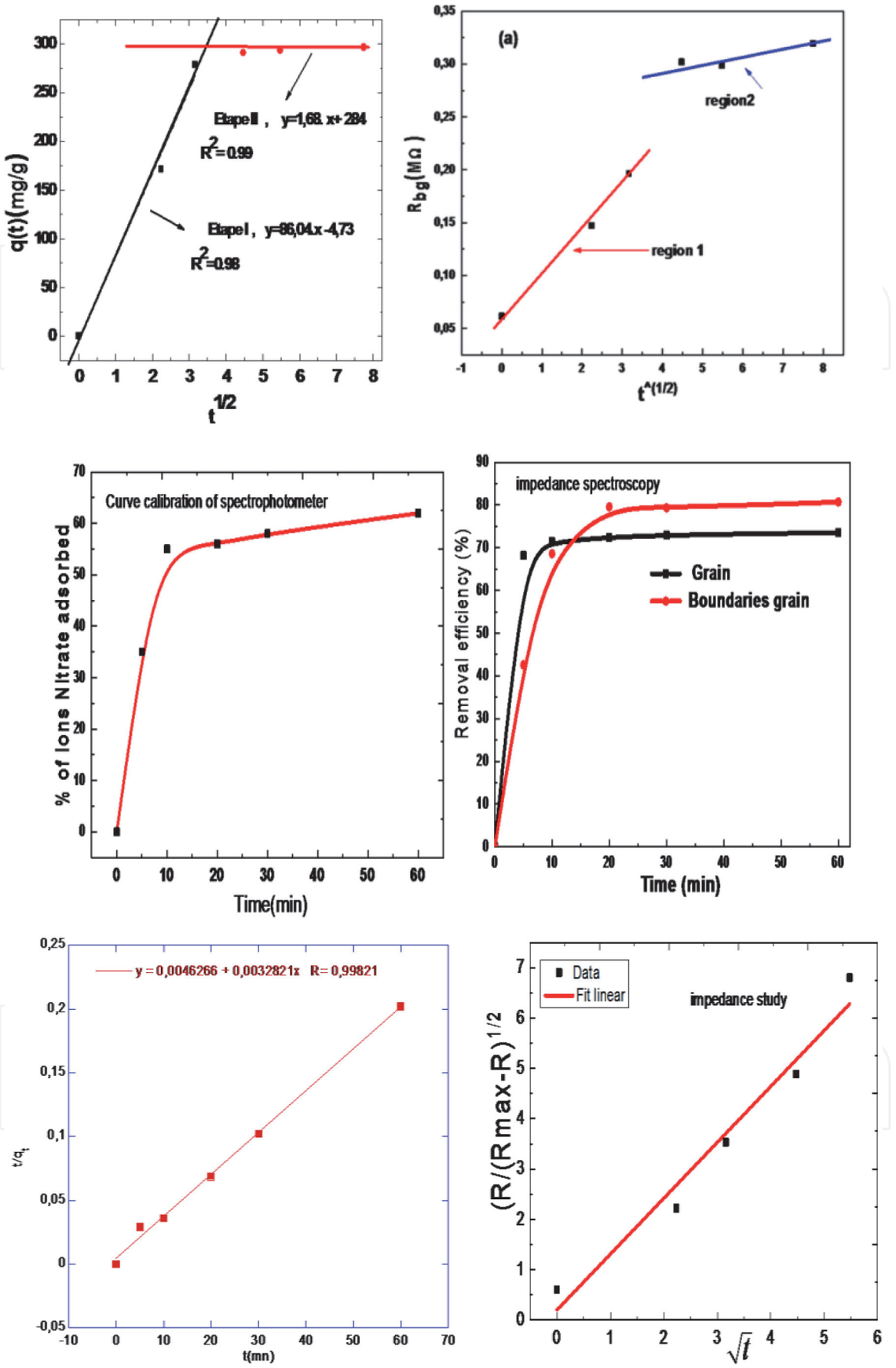

Figure 20.
Correlation figures between the kinetic and impedance spectroscopy studies of adsorption.

The distinction between kinetic and complex impedance spectroscopy study later controls the magnitude of the grain and the grain boundary and with a typical bulk permittivity in the range 103 to 105 using the relation and

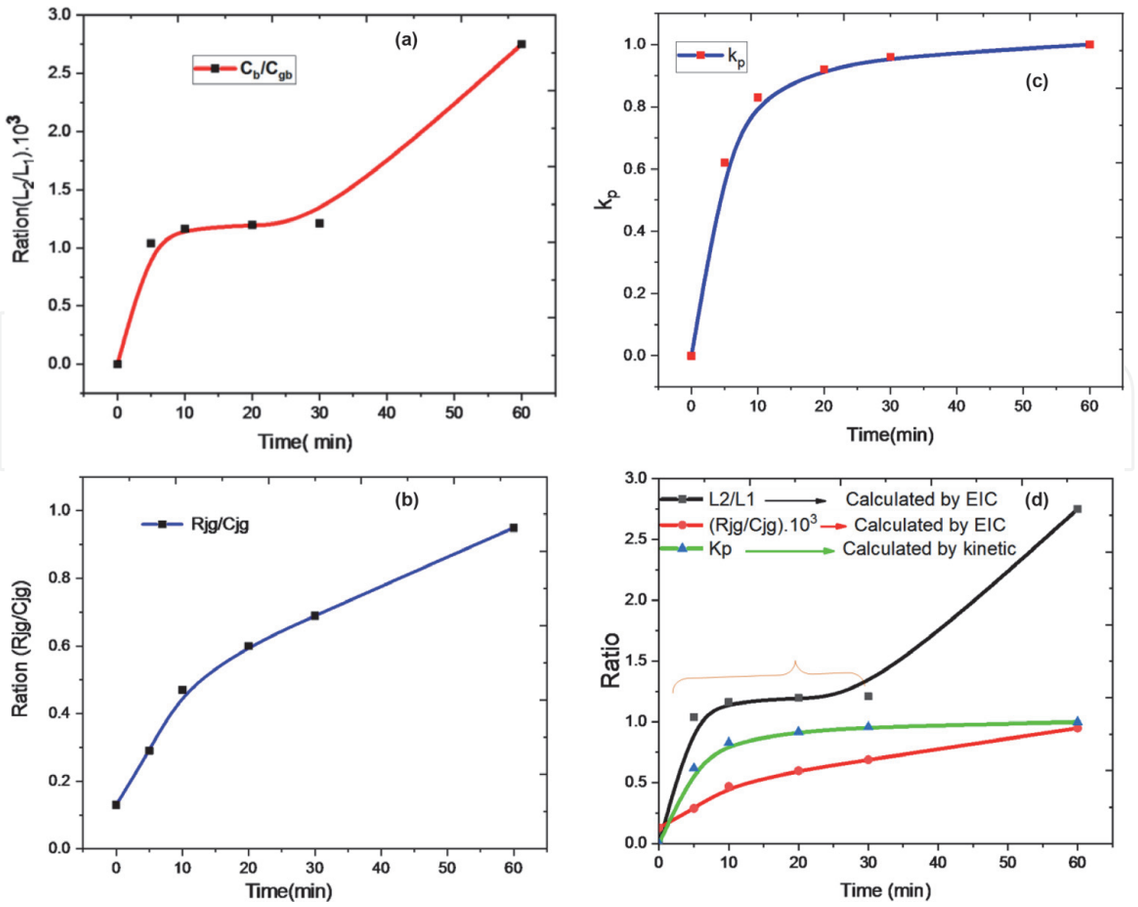

Figure 21.
(a) Ratio dimensional between grain and grain boundaries as a function of adsorption time. (b) Variation the fractality of system versus adsorption time. (c) Evolution of the partition coefficient between absorbance and absorbance as a function of time. (d) Variation in a comparative study between impedance spectroscopy and the kinetic study indicating the adsorption equilibrium.

visualized in **Figure 17** show the variation of imaginary part of permittivity at 1 kHz the frequency.

5. Conclusion

Characteristic band of NO_3^- and LDH, which indicated to the intercalating process, has been successful in the FT-IR diagram. Dielectric response of Zn_3-Al-Cl-LDH samples has been explained using the Cole-Cole presentation during the adsorption phenomenon. The resistor of the sample increased from 73,215 to 363,094 Kohms, and also the conductivity spectra exhibited high conductivity in high frequency according to two mechanisms of hopping conduction: one of the water molecules and the other of the nitrate ions adsorbed in the LDH. The mathematical fitting obtained using the equivalent circuit of these diagrams was carried out to obtain the conductivity following the double power law of Jonscher.

Acknowledgements

The author would like to thank the reviewers for their insight and their painstaking.

Funding statement

This research did not receive any specific grant from funding agencies in the public, commercial or not-for-profit sectors.

Competing interest statement

The authors declare no conflict of interest.

Additional information

No additional information is available for this paper.

Author details

Abderrahmane Elmelouky*, Abdelhadi Mortadi, Elghaouti Chahid and Reddad Elmoznine
Laboratory Physics of Condensed Matter, University Chouaib Doukkali, El Jadida, Morocco

*Address all correspondence to: elmlouky_abderrahmane@yahoo.fr

References

[1] Jeong JY, Kim HK, Kim JH, Park JY. Electrochemical removal of nitrate using ZVI packed bed bipolar electrolytic cell. Chemosphere. 2012;**89**:172-178. DOI: 10.1016/j.chemosphere.2012.05.104

[2] Zhou M, Fu W, Gu H, Lei L. Nitrate removal from groundwater by a novel three-dimensional electrode biofilm reactor. Electrochimica Acta. 2007;**52**:6052-6059. DOI: 10.1016/j.electacta.2007.04.010

[3] Thomson TS. Nitrate concentration in private rural drinking water supplies in saska Tchewan Canada. Bulletin of Environmental Contamination and Toxicology. 2001;**66**:64-70. DOI: 10.1007/s001280000206

[4] Majumdar D, Gupta N. Nitrate pollution of groundwater and associated human health disorders. Indian Journal of Environmental Health. 2000;**42**:28-39. DOI: 10.4236/jeas.2015.54015

[5] Tate CH, Arnold KF. Health and aesthetic aspects of water quality. In: Pontius FW, editor. Water Quality and Treatment. New York: McGraw-Hill Inc.; 1990. pp. 63-156

[6] Zheng Y, Wang A. Nitrate adsorption using poly (dimethyl diallyl ammonium chloride)/polyacryl amide hydrogels. Journal of Chemical & Engineering Data. 2010;**55**:3494-3500. DOI: 10.1021/je100169r

[7] Chatterjee S, Woo SH. Removal of nitrate from aqueous solutions by chitosan hydrogel beads. Journal of Hazardous Materials. 2008;**164**:1012-1018. DOI: 10.1016/j.jhazmat.2008.09.001

[8] Reichel WT. Synthesis of anionic clay minerals. Solid State Ionics. 1986;**22**:135-142. DOI: 10.1016/0167-2738 86) 90067-6

[9] El Ouardi M, Qourzal S, Alahiane S, Assabbane A, Douch J. Effective removal of nitrates ions from aqueous solution using new clay as potential low-cost adsorbent. Journal of Encapsulation and Adsorption Sciences. 2015;**05**(04):178-190. DOI: 10.4236/jeas.2015.54015

[10] Wakelin SA, Colloff MJ, Kookanal RS. Effect of wastewater treatment plant effluent on microbial function and community structure in the sediment of a freshwater stream with variable seasonal flow. Applied and Environmental Microbiology. 2008;**74**:2659-2668. DOI: 10.1128/AEM.02348-07

[11] Dabrowski A. Adsorption—From theory to practice. Advances in Colloid and Interface Science. 2001;**93**:135-224

[12] Bates JB, Chu YT, Stribling WT. Surface topography and impedance of metal electrolyte interfaces. Physical Review Letters. 1988;**60**:627

[13] Horvat-Radosevic V, Kvastek K. Hydrogen/anion electro sorption at rhodized electrodes as revealed by electrochemical impedance spectroscopy. Journal of Electroanalytical Chemistry. 2004;**566**:451-465

[14] Yoo HD, Jang JH, Ka BH, Rhee CK, Oh SM. Impedance analysis for hydrogen adsorption pseudo capacitance and electrochemically active surface area of Pt electrode. Langmuir. 2009;**25**(19):11947-11954

[15] Barbero G. Influence of adsorption phenomena on the impedance spectroscopy of a cell of liquid. Physical Review E. 2005;**71**:062201

[16] Barbero G, Becchi M, Strigazzi A, Digabel JL, Neto AMF. Experimental evidence for the adsorption-desorption phenomena on the spectroscopy impedance measurements of an

electrolytic cell. Journal of Applied Physics. 2007;**101**:044102

[17] Bataliotoa F, Martins OG, Duarte AR, Neto AMF. The impudence of adsorption phenomena on the impedance spectroscopy of an electrolytic cell. European Physical Journal E: Soft Matter and Biological Physics. 2011;**34**:10

[18] Nakanishi M. Graphical conversion between compliance and modulus, permittivity and electric modulus, impedance and admittance. International Journal of Spectroscopy. 2014:7. DOI: 10.1155/2014/538206. Article ID 538206

[19] El Melouky A, El Moznine R, Lahkale R, Sadik R, Sabbar E, Chahid E, et al. Journal of Optoelectronics and Advanced Materials. 2013:1239-1247

[20] Ahmed AAA, Talib ZA, Zobir Bin Hussein M, Zakaria A. Solid State Sciences. 2012:1196-1202

[21] Yadav AK, Akashi CP, Haritash AK, Kansal A, Rani N. Journal of Hazardous Materials. 2006;**128**:289-293

[22] Yang L, Maomao Yang ID, Xu P, Zhao X, Bai H, Li H. Characteristics of nitrate removal from aqueous solution by modified steel slag. Water. 2017;**9**: 757. DOI: 10.3390/w9100757

[23] Ahmed AAA, Talib ZA, Zobir Bin Hussein M, Zakaria A. Journal of Solid State Chemistry. 2012;**191**:271-278

[24] Reinhardt C. Weinheim (Federal) Germany: VCH Verlags y Eseuscha. D-6940. pp. 75–78

[25] Lagergren S. ZurTheorie der Sogenannten Adsorption Gelöster Stoffe. Kungliga Svenska Vetenskap sakademiens. Handling 1898;**24**:1–39 (IGermany)

[26] Ho YS, Mckay G. Sorption of dye from aqueous solution by peat. Chemical Engineering Journal. 1998;**70**: 115-124

[27] Hamou RF, Macdonald JR, Tuncer E. Dispersive dielectric and conductive effects in 2D resistor-capacitor networks. Journal of Physics: Condensed Matter. 2009;**21**:025904

[28] Randles JEB, Somerton KW. Transactions of the Faraday Society. 1952;**48**:937-950

[29] Zhu X-h, Li J, Jin Y, Guo Y-h. Preparation of porous hybrid adsorbents based on fluor(calcium silicate)/ activated carbon and its application in the removal of iron (III) from ammonium phosphate solutions. Arabian Journal of Chemistry. 2018. DOI: 10.1016/j.arabjc.2017.12.006

[30] Funke K. Solid State Chemistry. 2007;**22**:111

[31] K. Zhao. Chemical Industry Press. Beijing. 2008

[32] Lv L, He J, Wei M, Evans DG, Duan X. Water Research. 2006;**40**(4): 735-743

[33] Abe M, Ogino K. Journal of Colloid and Interface Science. 1981;**80**:58-66

[34] Ismaïli M, Bougroua F, Isaert N, Legrand C, Nguyen HT. Physical Review E. 2001;**65**:011701

[35] Islam M, Patel R. Synthesis and physicochemical characterization of Zn/Al chloride layered double hydroxide and evaluation of its nitrate removal efficiency. Desalination. 2010;**256**:120

[36] Senthil Kumar P, Sakunthala A, Prabu M. Impact of cerium doping on the structural and electrical properties of lithium nickel manganese oxide ($LiNi_{0.5}Mn_{0.5}O_2$). International Journal of ChemTech Research. 2014;**6**: 5252-5255

[37] Córdoba-Torres P. Characterization of frequency dispersion in the impedance response of a distributed model from the mathematical properties of the distribution function of relaxation times. Electrochimica Acta. 2015;**180**: 591

[38] Liang P, Yang Z, Chao X. Journal of Alloys and Compounds. 2016;**678**: 273-283

[39] El Moznine R, Smith G, Polygalov E, Suherman PM, Broadhead J. Journal of Applied Physics. 2003;**36**:330-333

[40] Roto R, Villemure G. Journal of Electroanalytical Chemistry. 2002;**527**: 123-130

[41] Gupta SS, Bhattacharyya KG. Advances in Colloid and Interface Science. 2011;**162**:39-58

[42] Badapanda T, Senthil V, Rout SK, Cavalcante LS, Simões AZ, Sinha TP, et al. Current Applied Physics. 2011;**11**: 1282-1293

[43] Hajra S, Sahoo S, Mishra T, De M, Rout PK, Choudhary RNP. Journal of Materials Science: Materials in Electronics. 2018;**29**:7876-7884. DOI: 10.1007/s10854-018-8787-8

[44] Mehrotra V, Giannelis EP. Journal of Applied Physics. 1992;**72**:1039-1048

[45] Elhatimi W, Lahkale R, Bouragba FZ, Sadik R, Lebbar N, Elmelouky A, et al. Journal of Spectroscopy Letters. 2017

[46] Liang X, Hou W, Xu Y, Sun G, Wang L, Sun Y. Physicochemical and Engineering Aspects. 2010;**366**:50-57

[47] Ho YS. Journal of Hazardous Materials. 2006;**136**:681-689

[48] Elmelouky A, Chahid E, Elmoznine R, Lahkale R, Sabbar E. Analysis of conduction mechanism in lamellar double hydroxide by impedance spectroscopy. Journal of Optoelectronics and Advanced Materials. 2013;**15**(11):1239-1247

[49] Ahmed AAA, Talib ZA, Bin Hussein MZ, Zakaria A. Influence of metallic molar ratio on the electron spin resonance and thermal diffusivity of ZnRAl layered double hydroxide. Journal of Solid State Chemistry. 2013: 271-278

[50] Liang PF, Zhu T, Fang Y, Li Y, Han Y, Wu Y, et al. Atmospheric Chemistry and Physics. 2017;**17**:13921-13940

[51] Lahkale R, Elhatimi W, Sadik R, Bouragba FZ, Lebbar N, El A, et al. Nitrate-intercalated $Mg_{1-x}Al_x$-layered double hydroxides with different layer charges (x): Preparation, characterization, and study by impedance spectroscopy. Applied Clay Science. 2018;**158**:55-64

[52] Elhatimi W, Bouragba FZ, Lahkale R, Sadik R, Lebbar N, Siniti M, et al. Solid State Sciences. DOI: 10.1016/j.solidstatesciences.2018.03.006

[53] Elmelouky A, Mortadi A, Chahid E, Elmoznine R. Impedance spectroscopy as a tool to monitor the adsorption and removal of nitrate ions from aqueous solution using zinc aluminum chloride anionic clay. Heliyon. 2018;**4**. DOI: 10.1016/j.heliyon.2018.e00536